Bioactive triterpenoids isolated and characterized from Ficus sur (Forrsk) stem bark extract demonstrate inhibitory activity against benign prostatic hyperplasia protein targets using in silico study

Uchenna Benjamin Okeke

okeke.uchenna@abuad.edu.ng

Afe Babalola Universi

Patrick Igbinaduwa

University of Benin

Ibrahim Oluwatobi Kehinde

University of KwaZulu-Natal

Vuyisa Mzozoyana

University of KwaZulu-Natal

Research Article

Keywords: Ficus sur, amyrin acetate, sitosterol, prostatic hyperplasia, triterpenoid

Posted Date: March 6th, 2026

DOI: https://doi.org/10.21203/rs.3.rs-8786768/v1

Additional Declarations: No competing interests reported.

Abstract

Plants possess an abundant reservoir of compounds that can be harnessed and repurposed as therapeutic agents for the management of existing and emerging disease conditions, such as benign prostatic hyperplasia (BPH). This study aimed to isolate and characterize bioactive phytochemicals from the ethyl acetate fraction of *the Ficus sur* hydroethanol stem bark extract (FSSE) and to carry out *in silico* evaluation of their activity against key protein targets implicated in BPH pathogenesis. *Ficus sur* stem bark was collected from its natural habitat, authenticated, extracted, and partitioned into different solvent fractions (dichloromethane, ethyl acetate, and *n*-butanol). Sequential open column chromatography and preparatory thin layer chromatography of the ethyl acetate fraction led to the isolation and purification of compounds, which were characterized by spectroscopic analysis (UV, FTIR, ^{1}H and ^{13}C-NMR, and DEPTQ experiments). An *In-silico* molecular docking study was conducted using Autodock Vina, while ADMETlab 3.0 was employed to predict the physicochemical properties and drug-likeness of the isolated compounds. Two triterpenoids, α-amyrin acetate (110 mg) and β-sitosterol (340 mg), from the eight isolated compounds were characterized. *In silico* analyses indicated that both compounds exhibited binding affinities and physicochemical profiles comparable to those of the co-crystallized ligand finasteride across the four molecular targets implicated in benign prostatic hyperplasia. This gave credence to the medicinal richness of this plant and its use in folklore for urinary-related disorders such as BPH. It has been established in this study that *F. sur* stem bark extract is rich in bioactive compounds that can be explored for the discovery of leads for developing new drug candidates, especially for BPH management.

1 Introduction

The search for chemical entities from natural products for the management of emerging and complex disease conditions has continued to experience a quantum leap, creating a basis for more extensive scientific exploration of diverse lead structures that serve as templates for developing new pharmaceuticals. The growing interest in herbal medicines is largely driven by the perception that they are safer and more affordable than synthetic drugs, which are often expensive and associated with adverse side effects. Studies have revealed that various phytochemicals, such as alkaloids, flavonoids, phenolics, terpenoids, and saponins, found in medicinal plants can trigger a range of biological activities in living organisms, including antioxidant, anti-inflammatory, antibacterial, antiviral, and antitumor effects (Zhang et al., 2024). In vitro and in vivo studies validated these hypotheses that plant-derived compounds act through multiple pathways (Latif and Nawaz, 2025), including inhibition of 5α-reductase, a key enzyme in benign prostatic hyperplasia and prostate cancer pathogenesis, due to their structural similarity to endogenous receptor ligands (Nguyen et al., 2024).

Benign prostatic hyperplasia (BPH), a nonmalignant enlargement of the prostate causing lower urinary tract symptoms (LUTS), has become a significant health issue among aging men worldwide (Speakman et al., 2015). Due to the bothersome side effects linked to conventional medications, the demand for herbal treatments for BPH management has greatly increased. Herbal remedies, some available in

formulated dosage forms, have demonstrated effectiveness in treating BPH, cancer chemotherapy, and chemoprophylaxis. For example, herbal preparations containing either single or combined extracts of *Saw palmetto, Serenoa repens, Pygeum africanum, Urtica dioica, Cucurbita pepo*, and β-sitosterol from *Hypoxis rooper* (African star grass) help manage BPH (Csikós et al., 2021).

Biological activity-guided isolation techniques have produced important therapeutic agents for diseases like cancer, Alzheimer's disease, infections, malaria, and diabetes (Atanasov et al., 2021). Advances in computer-aided drug design have further sped up the discovery and development of plant-derived drugs, making them increasingly promising. To achieve significant improvements and increase cost-efficiency in drug development, employing computational methods has become essential. Typically, after identifying and selecting disease-related targets, various computational tools perform key drug discovery steps, including target identification (such as an enzyme or protein receptor), modifying drug-like compounds, and optimizing these compounds to develop effective drug candidates (Duffy et al., 2012).

Ficus sur, also known as broom cluster fig or cape fig, belongs to the genus Moraceae and is widely distributed in several tropical African countries. The plant, due to its high medicinal richness, has been used in ethnomedicine to treat various disease conditions such as infections, tumors, pains, and urinary disorders (Sieniawska et al., 2022). Several phytochemicals, such as triterpenoids, polyphenols, and fatty acids, have been isolated from different parts of *F.* sur in preceding studies (Ogunlaja, 2022; Sieniawska et al., 2022). Several phytosterol (β-sitosterol, stigmasterol), oleanane-type (12-oleanen-3-yl acetate, oleanen-3-yl acetate), and ursine-type (urs-12-en-24-oic acid, α-amyrin, 3-acetoxy-α-amyrin) triterpenoids have been isolated from the latex, leaf, and stem bark of *F. sur* (Nwanisobi et al., 2021; Ogunlaja et al., 2022; Sieniawska et al., 2022; Mouelle et al., 2025). Okeke et al (2026) reported the presence of gamma-sitosterol from the *F. sur* hydroethanolic stem bark extract. However, there is a paucity of scientific validation of the efficacy of these phytochemicals on benign prostatic hyperplasia. This work reports herein the isolation and characterization of two triterpenoids, α-amyrin acetate and β-sitosterol, from the ethyl acetate fraction of the hydroethanolic stem bark of *F. sur* and *in silico* evaluation of their ameliorating activity against protein targets implicated in BPH pathogenesis.

2 Materials and Methods

2.1 Collection, extraction, and fractionation of plant material

F. sur stem bark was identified and collected from its natural habitat in Ibadan, Oyo State, Nigeria (Fig. 1), by Dr. Akinniyi Samuel Odewo, a Taxonomist at the Forest Research Institute of Nigeria (FRIN), Ibadan, with compliance to WHO guidelines on good agricultural and collection practices for medicinal plants (World Health Organization, 2003). A herbarium specimen of the plant material (FHI113940) was deposited in the facility. The powdered stem bark (5 kg) was extracted by maceration with 80% ethanol at room temperature for 72 hours. The solution was filtered using Whatman No. 4 filter paper, and the

filtrate was concentrated to dryness under vacuum at 50°C using a rotary evaporator to afford *F. sur* hydroethanol stem bark extract (FSSE) (yield: 286 g, 5.72% $^{w}/_{w}$).

Employing the modified Kupchan method of solvent partitioning as described by Van-Wagenen et al. (1993), 250 g of the extract initially suspended in 200 mL of distilled water was transferred completely into a 2000 mL separating funnel and successively partitioned in the order: *n*-hexane (HEX), dichloromethane (DCM), ethyl acetate (EtOAc), and *n*-butanol (BuOH). The various fractions collected were concentrated under vacuum in a rotary evaporator to obtain the concentrates, which were then air-dried and weighed.

2.2 Isolation and purification of compounds

Firstly, the ethyl acetate fraction (40.00 g) of FSSE was adsorbed onto silica gel (20.00 g, 70–230 mesh size) in a mortar to form a slurry, which was then air-dried and loaded into a 50 x 10 cm glass column packed with 500 g of silica gel (70–230 mesh). Dichloromethane (100%) was used to pack the column before loading the sample. The column was eluted with gradient solvent systems of increasing polarity in the order: *n*-hexane, dichloromethane, and ethyl acetate. A total of 32 fractions were collected (250 mL each) until the compounds were completely eluted from the column. The fractions were monitored by thin-layer chromatography (TLC), and those with similar TLC profiles were pooled and reduced *in vacuo* at 45°C to obtain 7 fractions (FSE-1 to FSE-7). Fractions FSE-1 (1–5), FSE-2 (6–9), and FSE-4 (13–14) were subjected to a series of open column chromatography (CC) and preparative thin-layer chromatography (PTLC) using gradient solvent systems. The various sub-fractions obtained were monitored with TLC to confirm the presence of a single spot. The isolated compounds (C1 – C8) (Fig. 2) were identified by TLC and melting point determination. The structures of the compounds were elucidated through spectral analysis, including ultraviolet (UV), Fourier Transform Infrared (FTIR), ^{1}H and ^{13}C NMR, and DEPTQ spectroscopic experiments, and by comparing the spectral data with literature values.

2.3 Molecular docking of isolated compounds

The chemical structures of the isolated and characterized compounds were drawn using ChemDraw and converted to 3D structures. The compounds were optimized by correcting stereochemistry, removing duplicates, and adjusting protonation states to physiological pH (Omotuyi et al., 2021). Molecular docking was performed using AutoDock Vina (version 1.2.3) to predict the binding affinities and interaction modes of the compounds with the BPH-related protein targets: 5α-reductase 2 (5αR2; PDB ID: 7BW1), α_{1A}-adrenoceptor (ADRA1A; PDB ID: 7YMJ), phosphodiesterase-5 (PDE5; PDB ID: 2H42), and muscarinic M3 receptor (PDB ID: 5ZHP) (Fig. 3) (Eberhardt et al., 2021; Trott and Olson, 2010). Before docking, the prepared protein and ligand structures were converted into the PDBQT format using AutoDock Tools (ADT, version 1.5.7). Docking calculations were carried out for each protein target using the prepared ligands within the defined grid box. For each ligand, AutoDock Vina generated multiple binding poses ranked by predicted binding affinity (kcal/mol). Docking results were visualized and

analyzed for protein–ligand interactions using UCSF Chimera and BIOVIA Discovery Studio Visualizer (Pettersen *et al.*, 2004).

2.4 Drug-likeness and *in-silico* ADMET prediction analysis of isolated compounds

ADMETlab 3.0 Web tool (https://admetlab3.scbdd.com/) was used to predict the physicochemical properties, toxicity profile, and drug-likeness nature of the isolated compounds. The drug-likeness was evaluated based on the Lipinski rule, which is related to the compounds' predicted absorption, distribution, metabolism, and excretion (ADME) properties. Compounds with multiple violations are generally less likely to demonstrate favourable *in vivo* activity. Topological polar surface area (TPSA), another critical pharmacokinetic parameter, was also examined, as it predicts membrane permeability of polar atoms; optimal passive absorption typically falls within the range of 20–140 Å² (Fu et al., 2024).

3 Results and Discussion

Open column chromatography (CC) and PTLC separation methods on Silica gel afforded the isolation of majorly semi-polar constituents (C1 to C8) from the ethyl acetate fraction of FSSE. The structure of the isolated compounds was confirmed using various spectral analysis techniques like ¹H NMR, ¹³C NMR, DEPTQ, and comparison of the spectra data with those in the literature.

3.1 Physical characteristics and identification of isolated compounds

Compound C5

α-Amyrin acetate. Isolated and purified as a 240 mg white solid, soluble in 99% chloroform, with a melting point of 225–227°C and a positive Liebermann-Buchard test for steroids.

Spectral Analysis

UV-vis spectrum ($CHCl_3$ solvent) recorded λmax at 227 nm in chloroform. The FTIR spectrum showed absorption bands (in cm^{-1}) at 2952.1, 2911.1, 1733.2, 1244.9, and 1457.4, respectively. This reflects the presence of key functional groups in the compound. Pansare et al. (2021) reported a similar FTIR absorbance pattern for α-amyrin acetate.

The ^1H NMR spectrum ($CDCl_3$ solvent; 600 MHz NMR spectrometer) of C5 shown in Fig. 4, revealed various proton peaks as follows (δ in ppm): 5.18 (1H, *t*, H-12), 4.51 (1H, *t*, H-3), 2.30 (3H, *s*, H-2'), 2.01 (1H, *m*, H-20), 1.90 (2H, *t*, H-11), 1.63 (2H, *m*, H-2), 1. 61 (1H, *t*, H-9), 1.53 (2H, *t*, H-6). Notably, the deshielded vinyl protons H-12 and H-3 peaks appeared downfield as a triplet at 5.15 ppm and a doublet of doublets at 4.50, respectively. A sharp, intense singlet at 2.10 ppm corresponds to the three methyl protons of an acetate group, confirming the presence of an acetate moiety. These spectral features are

consistent with an ursane-type pentacyclic triterpenoid, in contrast to the oleanane-type (e.g., β-amyrin), with a H-12 proton resonating near 5.18 ppm. Eight methyl signals are clustered in a crowded upfield region between 0.65 and 1.20.

The ^{13}C NMR and DEPTQ spectra in Figs. 5 and 6 revealed a total of 32 carbon signals, categorized as eight methyl (-CH_3), nine methylene (-CH_2), seven methine (-CH), and seven quaternary (–C-) carbons, detailed as follows ($CDCl_3$ solvent; 600 MHz NMR spectrometer): δ ppm 170.95 (C-1'), 139.64 (C-13), 124.34 (C-12), 80.97 (C-3), 59.10 (C-18), 55.30 (C-5), 47.67 (C-9), 42.10 (C-14), 41.74 (C-8), 40.06 (C-22), 39.83 (C-1). The chemical shift values presented in Table 1 align closely with those reported for α-amyrin acetate by Okoye et al. (2014), indicating concordance between the observed and literature NMR spectra. A characteristic signal at 170.92 ppm indicates a carbonyl carbon (C = O) of an ester. Peaks observed downfield at 124.34 and 139.64 ppm correspond to the olefinic C-12 methine and C-13 quaternary carbons, respectively. The methine carbons C-18 and C-19 appeared downfield at 59.10 and 39.84 ppm. These assignments further support the characterization of the compound as an ursane-type triterpenoid, distinguishing it from the oleanane framework, which typically shows C-12 and C-13 resonance peaks near 121 and 145 ppm, and C-18 and C-19 signals nearly overlapping around 47–47.5 ppm (Okoye et al., 2014; Viet et al., 2021). ^{1}H-^{1}H COSY of C5 (Fig. 11) revealed cross-peaks indicating coupling between neighboring protons, particularly H-2 / H-3 (1.6 and 4.55 ppm), H-11 / H-12 (1.9 and 5.15 ppm), and H-12 / H-18 (5.15 and 1.2 ppm).

Table 1

^{13}C-NMR and ^{1}H-NMR data of **C5** and α-amyrin acetate from literature

Position	Chemical shift, δ (ppm) value		Chemical shift, δ (ppm) value		α-amyrin acetate (Okoye et al., 2014)
	Compound C5 (δ ppm)		Compound C5 (δ ppm)		
	^{1}H	^{13}C	^{1}H	^{13}C	^{13}C NMR
1					
2	1.63 *(m)*				
3	4.55 *(dd)*	80.95	4.56 *(dd)*	80.97	81.18
4					
5		55.30		55.30	55.46
6	1.53 *(t)*				
7					
8				39.67	39.83
9	1.61 *(t)*	47.68		47.68	47.84
10					
11	1.90 *(t)*		1.98		
12	5.15 *(t)*	124.34	5.18 *(t)*	124.34	124.5
13		139.64		139.64	139.8
14		42.10		42.10	42.10
15					
16					
17					
18		59.10		59.10	59.26
19		39.84			
20	2.01 *(m)*				
21					
22					
23					
24					

Position	Chemical shift, δ (ppm) value		Chemical shift, δ (ppm) value		α-amyrin acetate (Okoye et al., 2014)
	Compound C5 (δ ppm)		Compound C5 (δ ppm)		
	^{1}H	^{13}C	^{1}H	^{13}C	^{13}C NMR
25					
26					
27					
28					
29					
30					
1'		170.92		170.95	171.53
2'	2.1				

Chemical shift values expressed as parts per million (ppm); *s*- singlet, *d*- doublet, *t*- triplet, *dd*- doublet of a doublet, *m*- multiplet

Compound C8

β-Sitosterol. Isolated and purified as a 341 mg pale yellow crystalline solid, soluble in 99% chloroform, with a melting point of 136–138°C, and a positive Liebermann-Buchard test for steroids.

Spectral analysis: UV-vis spectrum ($CHCl_3$ solvent) recorded λmax at 260 nm, principally attributed to a single isolated double bond and the solvent effect (bathochromic shift) of chloroform. ^{1}H NMR spectrum ($CDCl_3$ solvent, 600 MHz NMR) revealed various proton peaks at different chemical shifts (δ in ppm) as follows: 5.3 (1H, *s*, H-6), 3.48 (1H, *m*, H-3), 2.2 (2H, *m*, H-2), 2.2 (2H, *m*, H-4), 1.9 (2H, *t*, H-7) (Fig. 7). Table 2 reveals chemical shift values that correspond closely with the β-sitosterol NMR spectrum documented by Ododo et al. (2016) and Javed et al. (2021), confirming NMR spectral consistency between the observed and literature values. A distinct multiplet peak at 5.36 ppm corresponds to the olefinic proton on carbon C-6. The deshielded hydroxyl group proton on carbon C-3 appears as a doublet of doublets at 3.49 ppm.

^{13}C NMR and DEPTQ spectra of compound C5 in Figs. 8 and 9, revealed a total of 29 carbon signals as six methyl ($-CH_3$), eleven methylene ($-CH_2$), nine methine (-CH) and three quaternary (-C-) carbons, detailed as follows (600 MHz, in $CDCl_3$ solvent) δ ppm: 140.76 (C-5), 129.30 (C-6), 71.81 (C-3), 56.89 (C-17), 56.79 (C-14), 50.1 (C-9), 45.87 (C-24), 42.33 (C-13), 42.3 (C-4), 40.47 (C-12), 37.20 (C-1), 36.51(C-10), 36.15 (C-20). ^{1}H-^{1}H COSY revealed cross-peaks indicating correlations between neighboring protons in

compound C8 (Fig. 12), particularly H-2 / H-3 (2.3 and 3.49 ppm), H-3 / H-4 (3.39 ppm and 2.29 ppm), and H-6 / H-7 (5.35 and 1.98 ppm).

Table 2

^{13}C-NMR and ^{1}H-NMR data of **C8** and β-sitosterol from literature

Position	Compound C8 chemical shift, δ (ppm)		β-Sitosterol (Javed et al., 2021)	β-Sitosterol (Ododo et al., 2016)	β-Sitosterol (Javed et al., 2021)	β-Sitosterol (Ododo et al., 2016)
	^{1}H	^{13}C	^{1}H NMR	^{1}H NMR	^{13}C NMR	^{13}C NMR
1		37.27		1.46 *(m)*	36.8	37.28
2	2.3 *(m)*			1.56 *(m)*	31.2	31.69
3	3.49 *(m)*	71.81	3.45	3.54 *(m)*	72.2	71.82
4	2.29 *(m)*	42.23 *(t)*		2.32 *(m)*	42.4	42.33
5	-	140.76	-	-	141.2	140.77
6	5.35 *(t)*	121.71	5.41	5.37 *(t)*	122.1	121.73
7	1.98 *(t)*	31.88		2.04 *(m)*	31.8	31.93
8		31.63		1.69 *(m)*	31.63	31.93
9		50.19		1.55 *(m)*	51.9	50.16
10		36.15		-	35.8	36.51
11				1.52 *(m)*	22.8	21.11
12		40.47		1.51 *(m)*	40.6	39.80
13		39.80		-	41.8	42.34
14		56.88		1.50 *(m)*	56.8	56.79
15		24.31		1.58 *(m)*	24.8	24.33
16				1.85 *(m)*	28.6	28.27
17		56.09		1.45 *(m)*	56.2	56.08
18			0.68	0.70 *(s)*	12.6	11.89
19			1.03	1.03 *(s)*	20.6	19.42
20		33.97		1.60 *(m)*	34.4	36.17
21			0.92	0.94 *(d)*	18.9	18.84
22		31.92		0.93 *(m)*	32.2	33.98
23		26.1		1.15 *(m)*	25.4	26.11
24		45.87		1.38 *(m)*	46.4	45.86

Position	Compound C8 chemical shift, δ (ppm)		β-Sitosterol (Javed et al., 2021)	β-Sitosterol (Ododo et al., 2016)	β-Sitosterol (Javed et al., 2021)	β-Sitosterol (Ododo et al., 2016)
	^{1}H	^{13}C	^{1}H NMR	^{1}H NMR	^{13}C NMR	^{13}C NMR
25		29.70		1.57 *(m)*	30.4	29.19
26			0.86	0.84 *(d)*	21.2	19.84
27			0.82	0.86 *(d)*	19.81	19.06
28		23.09		1.10 *(m)*	23.8	23.10
29			0.89	0.82 *(t)*	12.8	12.01
C-3 OH		-		1.98 *(s)*	-	-

Chemical shift values expressed as parts per million (ppm); *s*- singlet, *d*- doublet, *t*- triplet, *m*- multiplet

3.2 Molecular docking analysis of isolated bioactive compounds against BPH targets

The docking scores, representing the predicted binding free energies (kcal/mol) of α-amyrin acetate and β-sitosterol, isolated from the ethyl acetate fraction of FSSE, against key therapeutic targets implicated in benign prostatic hyperplasia (BPH), are presented in Table 3.

Table 3
Molecular docking scores (kcal/mol) of α-amyrin acetate and β-sitosterol against BPH targets

Compounds	5α reductase 2	α_{1A}-adrenoceptor	Phosphodiesterase-5	Muscarinic M3
	PDB ID: 7BW1	PDB ID: 7YMJ	PDB ID: 2H42	PDB ID: 5ZHP
α-Amyrin acetate (C5)	-10.2	-10.9	-9.8	-8.0
β-Sitosterol (C8)	-10.7	-8.0	-6.8	-7.7
PDB – Protein Data Bank				

3.3 Molecular interaction analysis of *Ficus sur* bioactive compounds with BPH target proteins

Figure 13 and 14 depicted the two-dimensional (2D) interaction profiles of the isolated compounds in Fig. 10, docked against the four major therapeutic targets of BPH. The visualized interactions highlight a combination of Van der Waals forces, π–π stacking, π–alkyl, alkyl, and hydrogen bonding, which collectively contribute to the stability and specificity of the ligand–receptor complexes, corroborating the

docking energy results in Table 3. α-Amyrin acetate complexes displayed dense networks of hydrophobic and aromatic interactions across all receptor pockets, indicating a strong binding affinity and multi-target potential. Within the 5α-reductase 2 complex (7BW1), α-amyrin acetate established extensive π–alkyl and alkyl contacts with residues such as Phe118, Arg114, Leu23, and Val24, while also forming Van der Waals interactions with Ala26 and Gly115, stabilizing the ligand within the hydrophobic catalytic channel of the enzyme. In the α_{1A}-adrenoceptor complex (7YMJ), the compound interacted prominently with Trp102, Tyr176, and Phe312 through π–π and hydrophobic contacts, suggesting a strong occupation of the receptor's transmembrane binding site that could contribute to adrenergic antagonism. Similarly, in the phosphodiesterase-5 (2H42) complex, α-amyrin acetate formed stabilizing interactions with Phe820, Met816, and Ala823, complemented by π–alkyl contacts that mimic known inhibitor binding patterns in the cGMP catalytic domain. For the muscarinic M3 receptor (5ZHP), α-amyrin acetate maintained π–π and Van der Waals interactions with residues Phe437, Arg109, and Asn107, suggesting that it may also influence bladder contractility through muscarinic receptor modulation. These interactions explain the consistently high docking energies observed (− 10.9 to − 8.0 kcal/mol) and reinforce the compound's potential as a multi-target modulator in BPH.

β-Sitosterol also exhibited favorable interaction patterns with all four BPH targets. In the 5α-reductase binding pocket, β-sitosterol engaged in π–π stacking and alkyl interactions with key hydrophobic residues, including Phe118, Tyr176, and Leu23, which are crucial for enzyme inhibition and suppression of dihydrotestosterone biosynthesis. The α_{1A}-adrenoceptor complex revealed π–alkyl interactions with Phe312 and Trp102, along with hydrogen bonding to Tyr196, which collectively suggest strong antagonistic behavior similar to known α1-blockers. Within the phosphodiesterase-5 complex, β-sitosterol interacted mainly with hydrophobic residues Phe820, Met816, and Val826, while the M3 receptor complex exhibited π–π stacking with Phe437 and hydrophobic contacts with Ile424 and Val426. The abundance of hydrophobic and aromatic contacts indicates that β-sitosterol's lipophilic nature allows it to efficiently stabilize within receptor pockets, consistent with its recognized pharmacological role as a 5α-reductase inhibitor and prostate health modulator.

The molecular interaction analysis confirms that the investigated phytoconstituents, α-amyrin acetate and β-sitosterol, exhibit strong and complementary binding profiles across multiple BPH-related targets. Their interactions are dominated by π–π and hydrophobic forces involving catalytically and structurally relevant residues, which not only stabilize the complexes but also suggest a synergistic multi-target therapeutic mechanism. This molecular evidence supports the hypothesis that the bioactive constituents of *Ficus sur* exert anti-BPH activity through concurrent inhibition of androgenic (5α-reductase), adrenergic (α_{1A}-adrenoceptor), phosphodiesterase (PDE-5), and muscarinic receptor pathways, offering a mechanistic rationale for the traditional use of *Ficus sur* in prostate and urinary-related disorders.

3.4 Drug-Likeness and ADMET Properties of Isolated Compounds

The drug-likeness and pharmacokinetic profile of α-amyrin acetate (C5) and β-sitosterol (C8) isolated from ethyl acetate fraction of FSSE were evaluated using the ADMETlab 3.0 web interface, with reference to Lipinski's rule of five (molecular mass (< 500 Da), lipophilicity (Log*P* ≤ 5), hydrogen bond donors (HBD ≤ 5), and hydrogen bond acceptors (HBA ≤ 10) (Lipinski et al., 2001), along with additional pharmacokinetic descriptors. Table 3 summarises the key parameters supporting the suitability of the isolated compounds for biological evaluation, including their predicted physicochemical properties, lipophilicity, water solubility, pharmacokinetics, and overall drug-likeness. α-Amyrin acetate and β-sitosterol demonstrated favourable oral bioavailability, obeying Lipinski's rule of 5. The ADMETLab output for the two compounds showed a coloured zone that represents the suitable physicochemical space for oral bioavailability, based on key physicochemical descriptors. Table 3 presents the critical parameters supporting Compounds C5 and C8 as candidates for biological evaluation. These features further suggest that both compounds are likely to demonstrate good oral bioavailability, which reinforces the potential of the compounds as therapeutic candidates for the treatment of BPH and other bladder disorders.

Table 3
ADMET physicochemical properties of ligands with the best binding affinities

Property	Meaning	Optimal Value	α-Amyrin acetate	β-Sitosterol
MW	Molecular weight	150 mg/mol ≤ MW ≤ 500 g/mol	468.4	414.39
LogP	Lipophilicity	0–3 log mol/L	*5.799	*8.004
LogS	Aqueous solubility	-4–0.5 log mol/L	-6.519	-7.221
LogD	Distribution coefficient (pH 7.4)	1–3 log mol/L (pH 7.4)	4.211	5.37
TPSA	Topological polar surface area	0 ~ 140A^2	26.3	20.23
nHA	Number of hydrogen bond acceptors	0 ~ 12	2.0	1.0
nHD	Number of hydrogen bond donors	0 ~ 7	0.0	1.0
nRot	Number of rotatable bonds	0 ~ 11	2.0	6.0
nRing	Number of rings	0 ~ 6	5.0	4.0
nRig	Number of rigid bonds	0 ~ 30	27.0	20.0
MaxRing	Number of atoms in the biggest ring	0–18	22.0	17.0
fCHar	Formal charge	-4 ~ 4	0.0	0.0
nHet	Number of heteroatoms	1 ~ 15	2.0	1.0
NLRV	Number of Lipinski's violations		1	1

* - **LRV**: Lipinski's rule violation; **NLRV**: Number of Lipinski's rule violations

4 Conclusion

Open column chromatography, preparative thin-layer chromatography, and instrumental analytical techniques such as UV, FTIR, ^{1}H and ^{13}C NMR, resulted in the isolation of an ursane-type pentacyclic triterpenoid, α-Amyrin acetate (C5), and a phytosterol, β-sitosterol (C8). Both compounds (α-amyrin acetate and β-sitosterol) exhibited ameliorative effects against BPH through molecular docking on BPH protein targets, with β-sitosterol displaying binding scores comparable to those of the standard BPH drug, finasteride. This study highlights the diversity of this plant, validation of its traditional use and potential as a source of lead compounds for developing therapeutics to treat BPH and other urinary-

related conditions, and contribution to improvement in public health strategies for managing BPH, especially in developing regions where access to standard therapies may be limited.

Declarations

Acknowledgments

The authors acknowledge the contributions of the Faculty of Pharmacy, University of Benin, Nigeria, and Afe Babalola University, Ado-Ekiti, Nigeria, for providing the facilities for conducting this research, and also the School of Chemistry and Physics, University of KwaZulu-Natal, Durban, South Africa, for providing the facilities for the NMR experiments.

Author Contributions

Uchenna Benjamin Okeke: Research concept development, data collection, analysis, manuscript draft preparation, review, and editing. Patrick Igbinaduwa: Research concept development, data analysis, and critical reading of manuscript. Vuyisa Mzozoyana: NMR analysis and data collection. Ibrahim Oluwatobi Kehinde: Bioinformatics analysis, article draft review, and editing.

Funding

The authors declare that no funds, grants, or other support were received during the research work and preparation of this manuscript.

Data Availability

The authors declare that the data supporting the findings of this study are available within the paper. Should any raw data files be needed in another format, the corresponding author, upon reasonable request and with the consent of the other authors of this research, shall make them available.

Consent for publication

The authors declare no conflict of interest. We confirm the publication of this article.

Competing Interests

The authors declare that they have no competing interests.

Ethics and consent to participate

Permissions or licences for plant collection and animal use are not applicable in this study, as the plant is common and non-endangered. *Ficus sur* herbarium specimen (Voucher number: FHI113940) was deposited at Forest Herbarium Ibadan (FHI), located in the Taxonomy Section of the Department of Forest Conservation and Protection, Forestry Research Institute of Nigeria (FRIN), Ibadan. The plant identifier and collector at FRIN is Dr. Akinniyi Samuel Odewo.

References

1. Atanasov AG, Zotchev SB, Dirsch VM, Supuran CT. Natural products in drug discovery: Advances and opportunities. Nat. Rev. Drug Discov. 2021;20(3):200-216. https://doi.org/10.1038/s41573-020-00114-z
2. Csikós E, Horváth A, Ács K, Papp N, Balázs VL, Dolenc MS, Kenda M, Glavač NK, Nagy M, Protti M, Mercolini L, Horváth G, Farkas Á. Treatment of Benign Prostatic Hyperplasia by Natural Drugs. *Molecules* 2021;26(23):7141. doi: 10.3390/molecules26237141.
3. Duffy BC, Zhu L, Decornez H, Kitchen DB. Early phase drug discovery: cheminformatics and computational techniques in identifying lead series. Bioorg. Med. Chem. 2012;20(18):5324-5342. doi: 10.1016/j.bmc.2012.04.062.
4. Eberhardt J, Santos-Martins D, Tillack AF, Forli S. AutoDock Vina 1.2.0: New Docking Methods, Expanded Force Field, and Python Bindings. *J. Chem. Inf. Model.* 2021;61(8):3891–3898. doi: 10.1021/acs.jcim.1c00203.
5. Fu L, Shi S, Yi J, Wang N, He Y, Wu Z, Peng J, Deng Y, Wang W, Wu C, Lyu A, Zeng X, Zhao W, Hou T, Cao D. ADMETlab 3.0: an updated comprehensive online ADMET prediction platform enhanced with broader coverage, improved performance, API functionality and decision support. *Nucleic Acids Res. 2024;*52(W1):W422–W431. doi: 10.1093/nar/gkae236.
6. Javed S, Mahmood Z, Khan KM, Sarker SD, Javaid A, Khan IH, Shoaib A. Lupeol acetate as a potent antifungal compound against opportunistic human and phytopathogenic mold Macrophomina phaseolina. *Sci. Rep.* 2021;11:8417. doi: 10.1038/s41598-021-87725-7.
7. Latif, R., Nawaz, T. Medicinal plants and human health: a comprehensive review of bioactive compounds, therapeutic effects, and applications. *Phytochem. Rev.* 2025. https://doi.org/10.1007/s11101-025-10194-7.
8. Lipinski CA, Lombardo F, Dominy BW, Feeney PJ. Experimental and computational approaches to estimate solubility and permeability in drug discovery and development settings. *Adv. Drug Deliv. Rev.* 2001;46(1-3):3-26. https://doi.org/10.1016/S0169-409X(96)00423-1
9. Mouelle ENM, Nsangou FM, Fofack HMT, Mboutchak D, Koliye PR, Ateba AB, Ntie-Kang F, Akone SH, Happi NE. *In Vitro* and *In Silico* Studies of the Biological Activities of Some Secondary Metabolites Belonging to *Ficus sur* Forssk (Moraceae): Towards Optimization of Wighteone Metabolite. *Chem. & Biodivers.* 2025;22(1):e202401270. https://doi: 10.1002/cbdv.202401270.
10. Nguyen NP, Le QG, Truong VN, Nguyen TND, Phan NTT, Tran MH. In vitro inhibition of 5-α reductase and in vivo suppression of benign prostatic hyperplasia by Physalis angulata ethyl acetate extract. *Fitoterapia*, 2024;175:105950. doi: 10.1016/j.fitote.2024.105950.
11. Nwanisobi GC, Aghanwa CI, Ezeagu CU. Fatty Acid Composition of *Ficus Sur* Seed Oil (Moraceae) Obtained in Enugu State, Nigeria. *J. Chem. Soc. of Nigeria* 2021;46(6):1055-1061. doi: 10.46602/jcsn.v46i6.686

12. Ododo MM, Choudhury MK, Dekebo AH. Structure elucidation of β-sitosterol with antibacterial activity from the root bark of Malva parviflora. *SpringerPlus* 2016;5(1):1210. https://doi.org/10.1186/s40064-016-2894-x
13. Ogunlaja OO, Moodley R, Baijnath H, Jonnalagadda SB. Antioxidant activity of the bioactive compounds from the edible fruits and leaves of *Ficus sur* Forssk. (Moraceae). *S. Afri. J. Sci.*2022;118(3/4). https://doi.org/10.17159/sajs.2022/9514.
14. Okeke UB, Igbinaduwa P, Aladesanmi JA, Mzozoyana V, Kehinde IO. GCMS-Based Phytochemical Profiling, Antioxidant and Anti-Inflammatory Activity of Triterpenoid-Rich Hydroethanolic Extract and Fractions of *Ficus Sur* (Forrsk) Stem Bark. *Nat. Life Sci. Commun.* 2026;(1):E2026012. DOI: 10.12982/NLSC.2026.012
15. Okoye NN, Ajaghaku DL, Okeke HN, Ilodigwe EE, Nworu CS, Okoye FB. beta-Amyrin and alpha-amyrin acetate isolated from the stem bark of Alstonia boonei display profound anti-inflammatory activity. *Pharm. Bio.* 2014;52(11):1478–1486. doi: 10.3109/13880209.2014.898078.
16. Omotuyi IO, Nash O, Ajiboye BO, Olumekun VO, Oyinloye BE, Osuntokun OT, Olonisakin A, Ajayi AO, Olusanya O, Akomolafe FS, Adelakun N. *Aframomum melegueta* secondary metabolites exhibit polypharmacology against SARS-CoV-2 drug targets: in vitro validation of furin inhibition. *Phytother Res.* 2021;35(2):908-919. https://doi: 10.1002/ptr.6843.
17. Pansare AV, Shedge AA, Sonawale MC, Pansare SV, Mahakal AD, Khairkar SR, Chhatre SY, Kulal DK, Patilb VR. Deciphering the interaction of a-Amyrin Acetate with hs-DNA: A multipronged biological probe. *RSC Adv.* 2021;12(3):1238-1243. https://doi.org/10.1039/D1RA07195E.
18. Pettersen EF, Goddard TD, Huang CC, Meng EC, Couch GS, Croll TI, Morris JH, Ferrin TE. UCSF ChimeraX: structure visualization for researchers, educators, and developers. *Protein Sci*. 2021;30(1):70–82. doi: 10.1002/pro.3943.
19. Sieniawska E, Świątek Ł, Sinan KI, Zengin G, Boguszewska A, Polz-Dacewicz M, Sadeer NB, Etienne OK, Mahomoodally MF. Phytochemical Insights into *Ficus sur* Extracts and Their Biological Activity. *Molecules* 2022;27(6):1863. doi: 10.3390/molecules27061863.
20. Speakman M, Kirby R, Doyle S, Ioannou C. Burden of male lower urinary tract symptoms (LUTS) suggestive of benign prostatic hyperplasia (BPH) - focus on the UK. *BJU Int.* 2015;115(4):508-19. https://doi.org/10.1111/bju.12745.
21. Trott O, Olson AJ. AutoDock Vina: improving the speed and accuracy of docking with a new scoring function, efficient optimization, and multithreading. *J Comput Chem.* 2010;31(2):455–461. https://doi.org/10.1002/jcc.21334.
22. *Van-Wagenen BC, Larsen R, Cardellina JH, Randazzo D, Lidert ZC, Swithenbank C. Ulosantion, a potent insecticide from the sponge Ulosa ruetzleri. J Org Chem. 1993;58:335–337.* https://doi.org/10.1021/jo00054a013.
23. Viet TD, Xuan TD, Anh LH. α-Amyrin and β-Amyrin Isolated from *Celastrus hindsii* Leaves and Their Antioxidant, Anti-Xanthine Oxidase, and Anti-Tyrosinase Potentials. *Molecules* 2021;26:7248. https://doi.org/10.3390/ molecules26237248.

24. World Health Organization. WHO guidelines on good agricultural and collection practices (GACP) for medicinal plants [internet]. Geneva; c2003 [cited 2023 Oct 16] Available from: https://iris.who.int/server/api/core/bitstreams/a00d3219-ed33-436a-be13-e3f00763f874/content
25. Zhang P, Wang H, Xu X, Ye Y, Zhang Y. Correlation analysis between phytochemical composition and biological activities of *Artemisia scoparia*. *Food Biosci.* 2024;62:105342. https://doi.org/10.1016/j.fbio.2024.105342.

Figures

Figure 1

Ficus sur in its natural habitat in Ibadan, Oyo, Nigeria

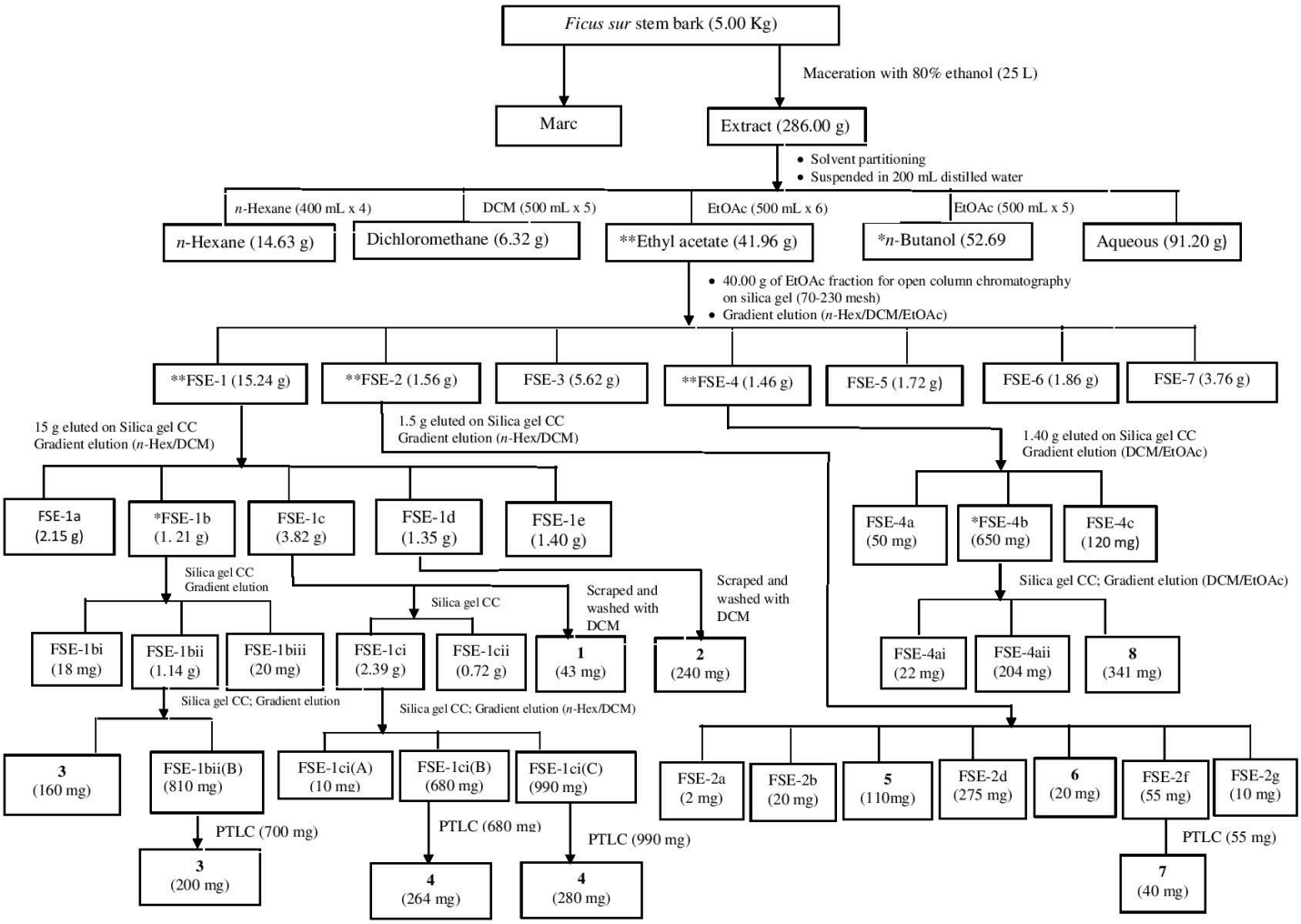

Figure 2

Flow chart for the activity-guided separation, isolation, and purification of bioactive compounds from *Ficus sur* hydroethanol stem bark extract

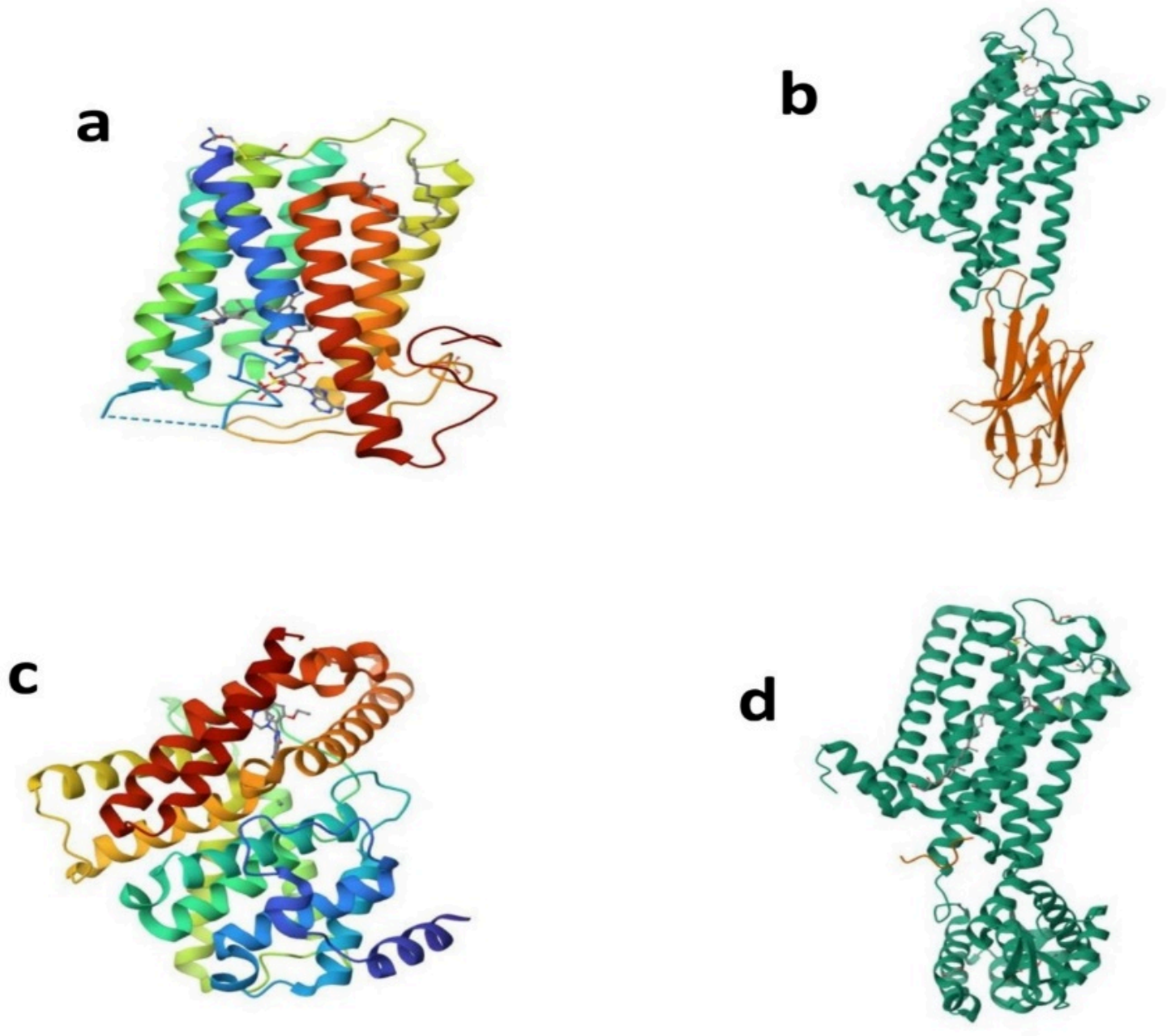

Figure 3

Crystal structures of: (a) Steroid 5-alpha-reductase 2 (PDB ID: 7BW1) in complex with Finasteride; (b) alpha-1_A adrenergic receptor R-Nb6 (PDB ID: 7YMJ) complex bound to tamsulosin; (c) Phosphodiesterase-5 (PDE5) (PDB ID: 2H42) in complex with sildenafil; and (d) the human M1 muscarinic acetylcholine receptor PDB ID: 5CXV) bound to antagonist tiotropium (https://www.rcsb.org/).

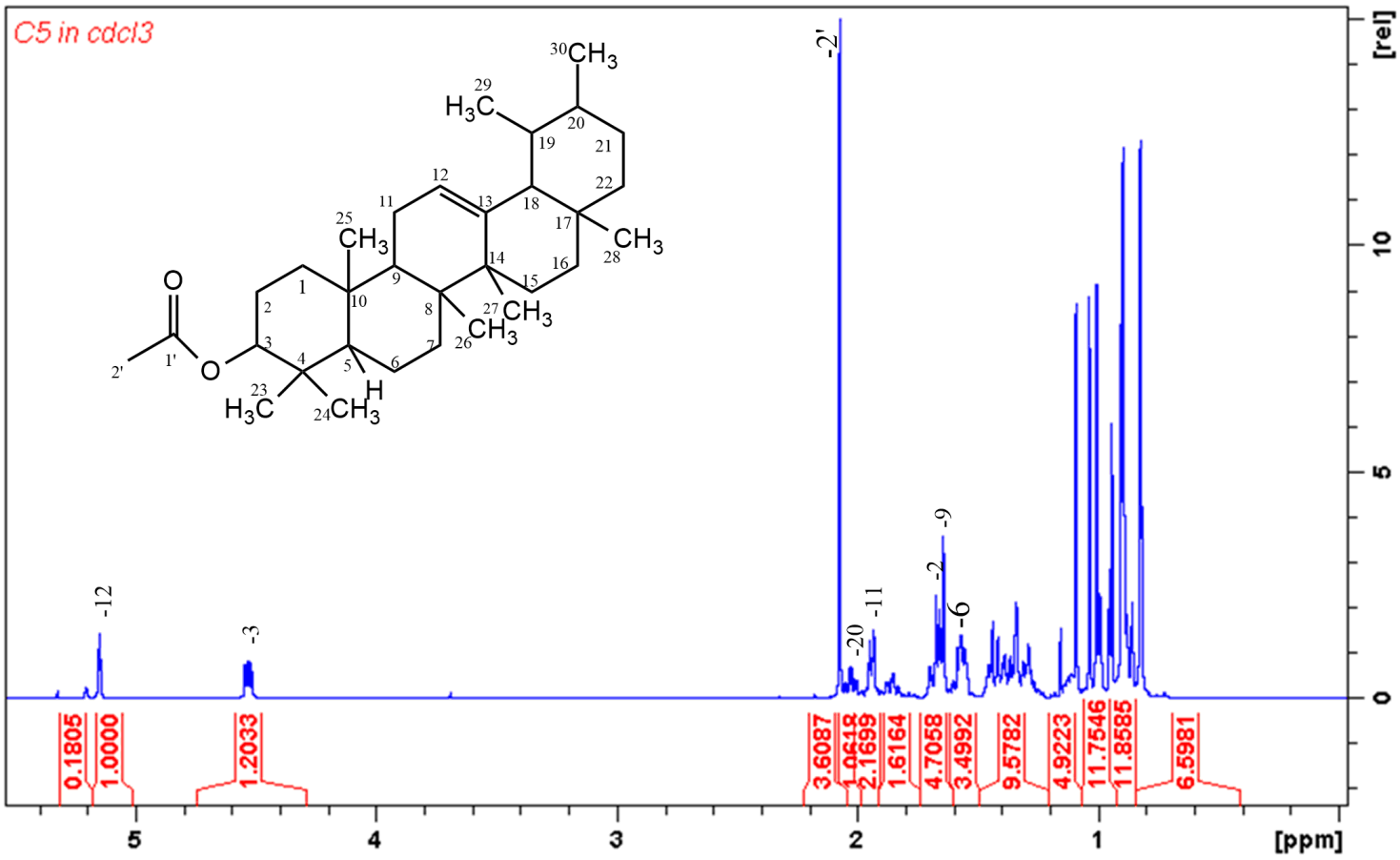

Figure 4

^{1}H-NMR spectrum of compound **C5**

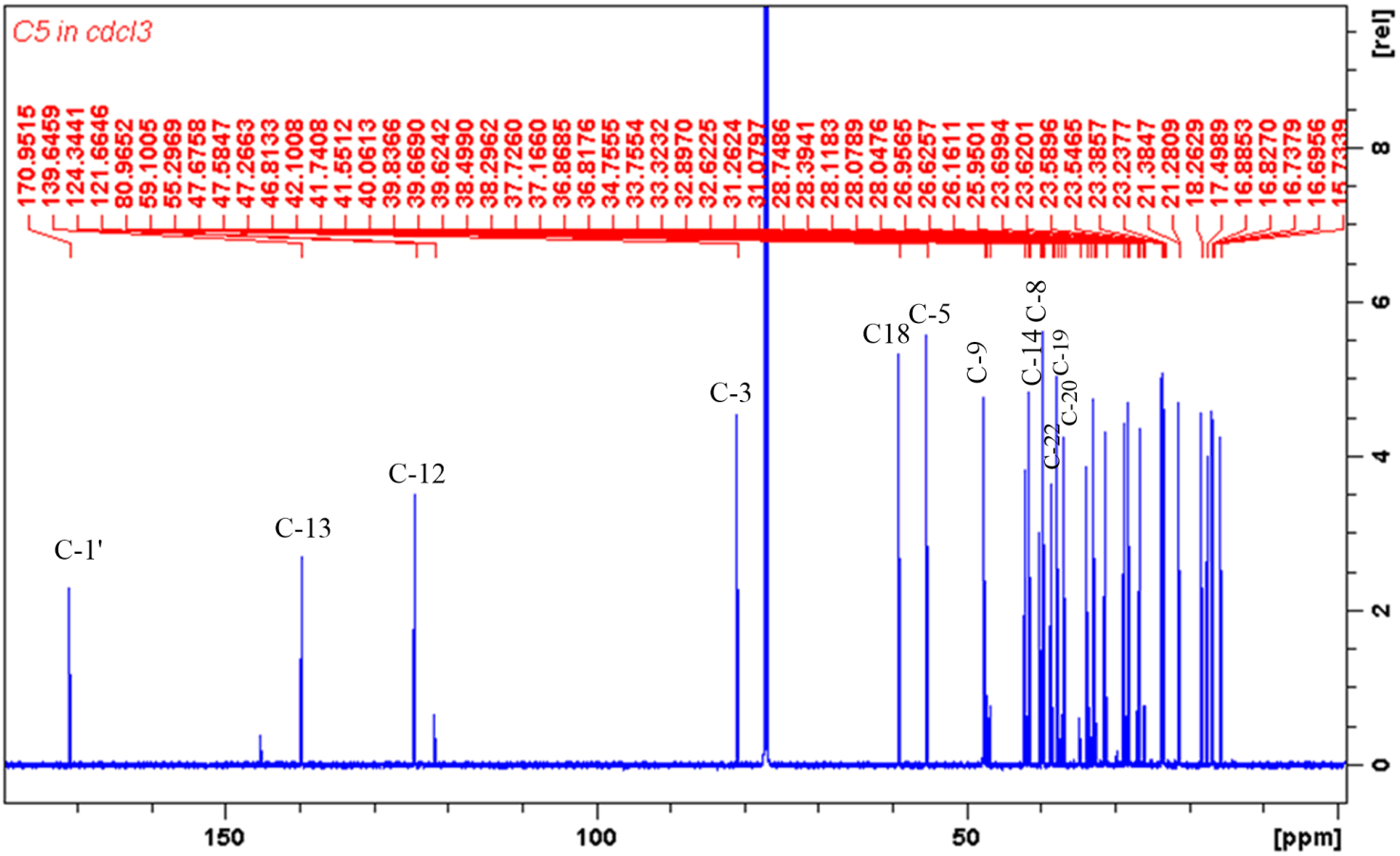

Figure 5

^{13}C-NMR spectrum of **C5** (600 MHz, $CDCl_3$) δ_{ppm}

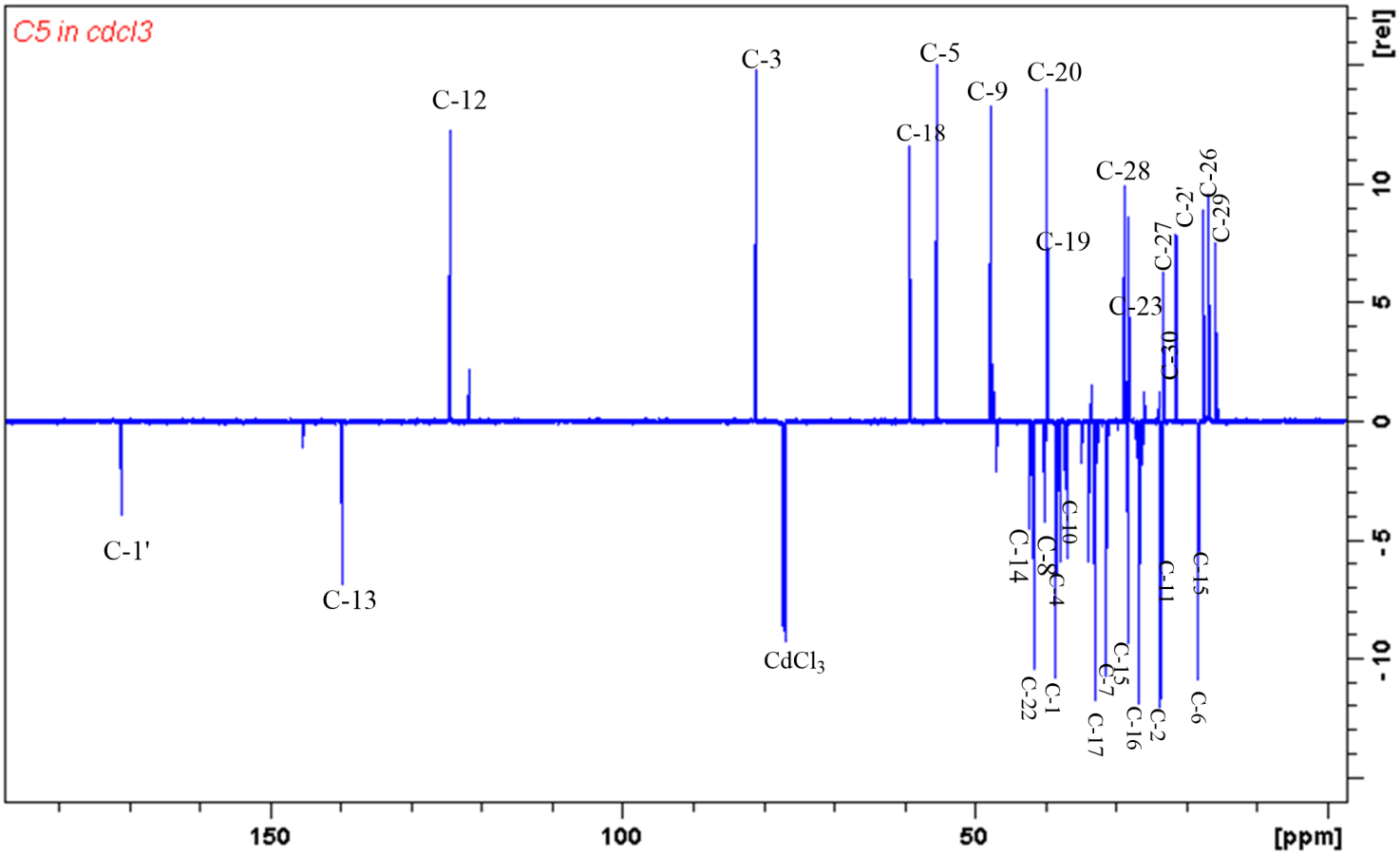

Figure 6

DEPTQ spectrum of compound **C5**

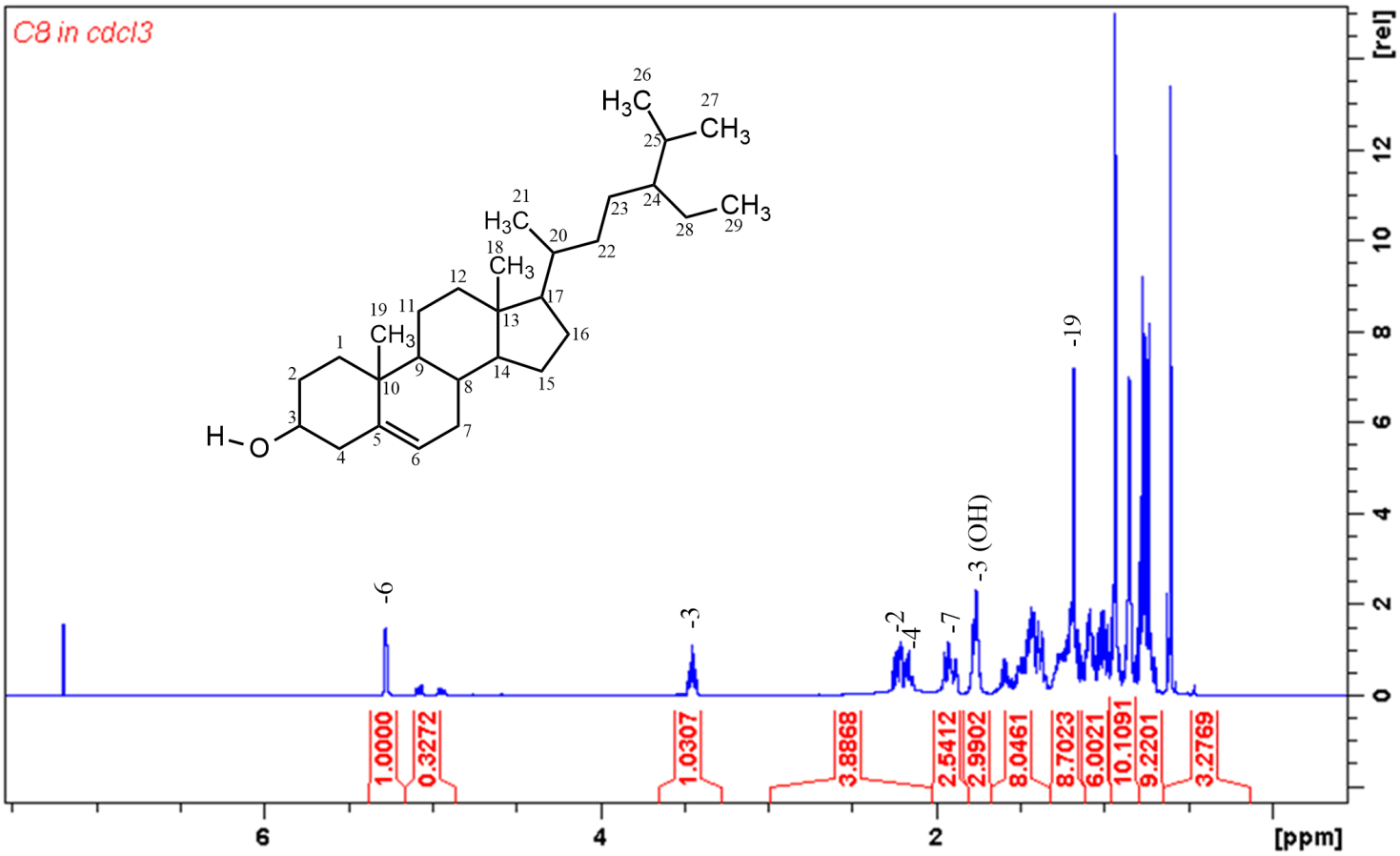

Figure 7

^{1}H-NMR spectrum of **C8** (600 MHz, $CDCl_3$) δ_{ppm}

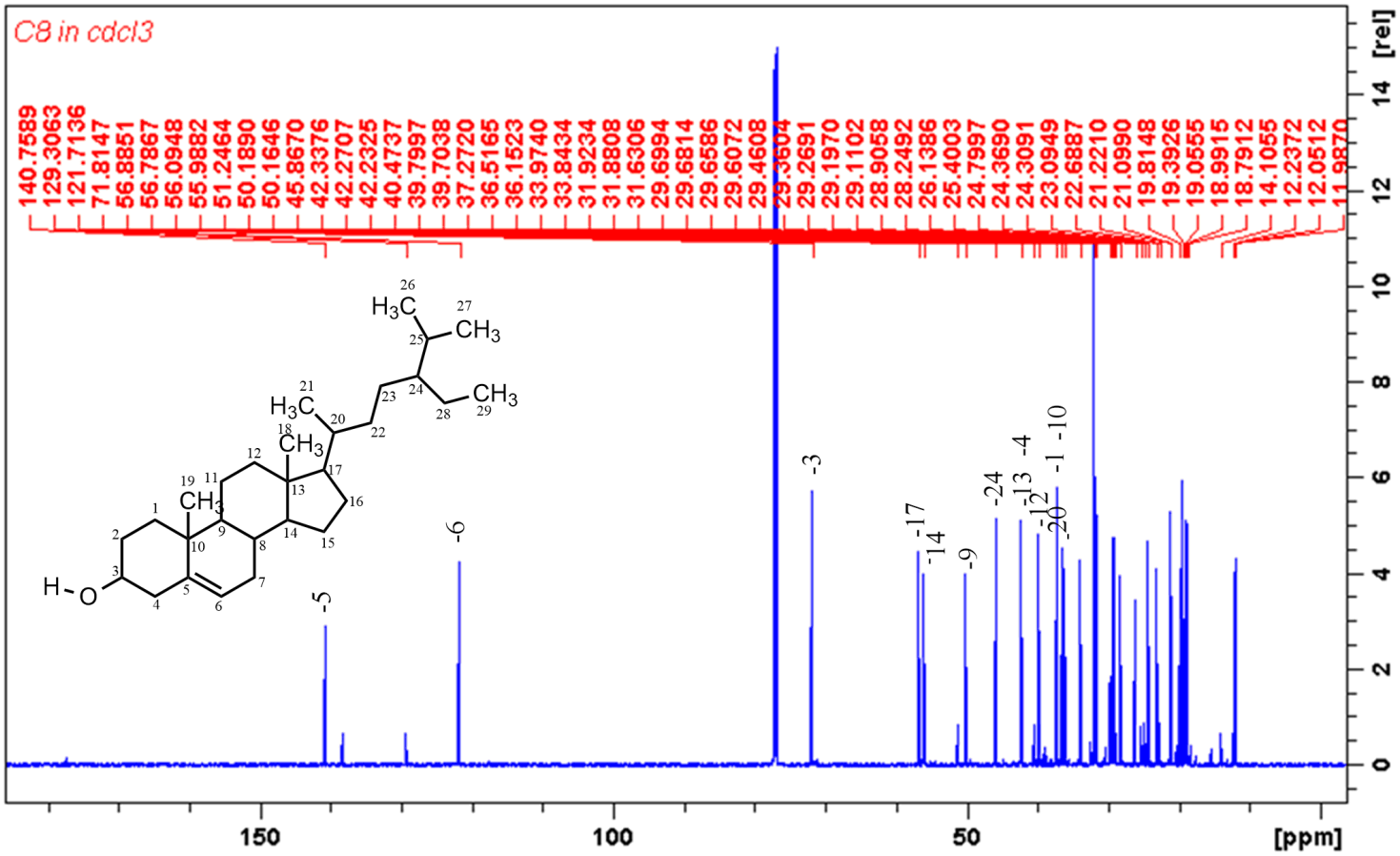

Figure 8

^{13}C-NMR spectrum of **C8** (600 MHz, $CDCl_3$) δ_{ppm}

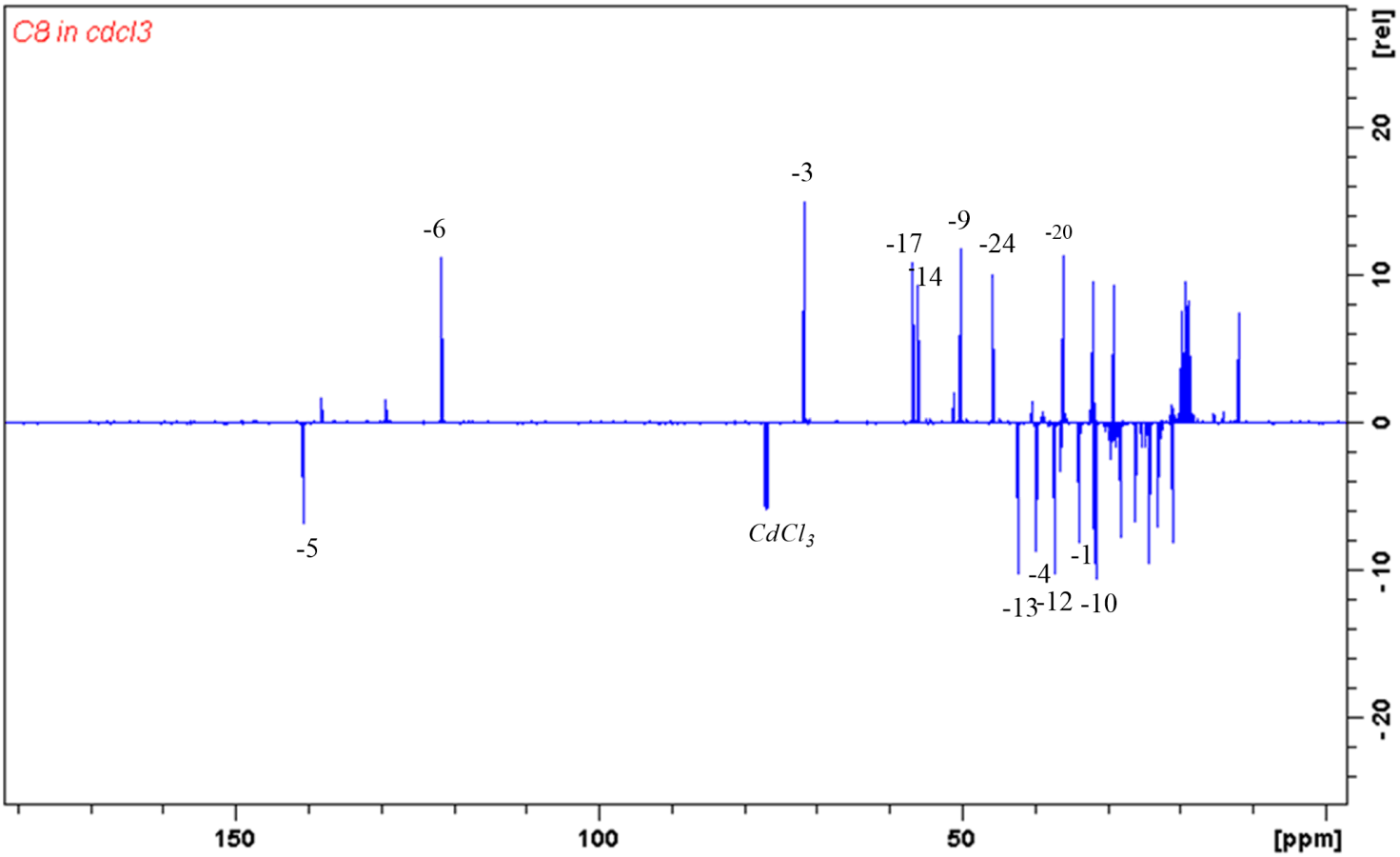

Figure 9

DEPTQ spectrum of compound **C8**

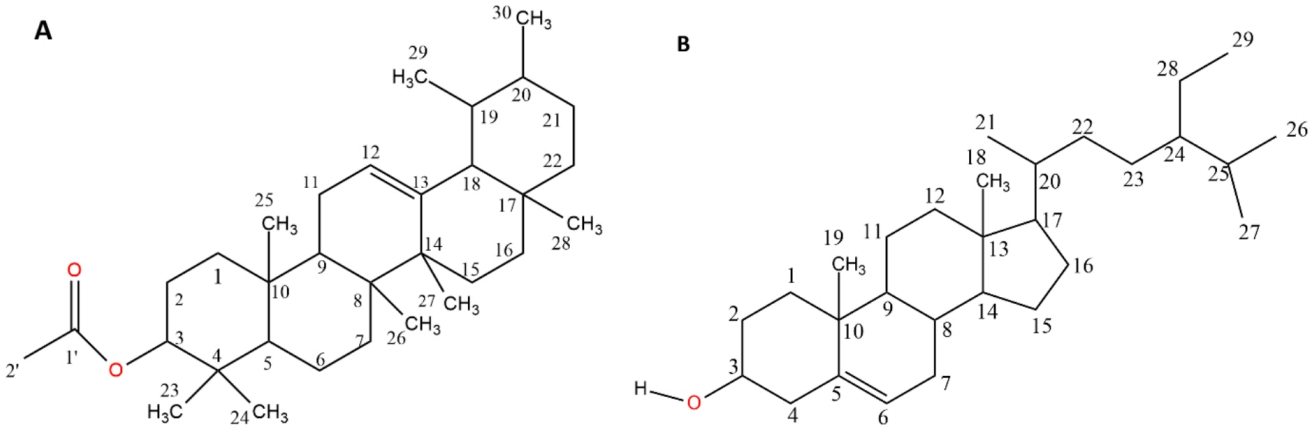

Figure 10

Structures of compound: (A) α-Amyrin acetate; (B) β-Sitosterol

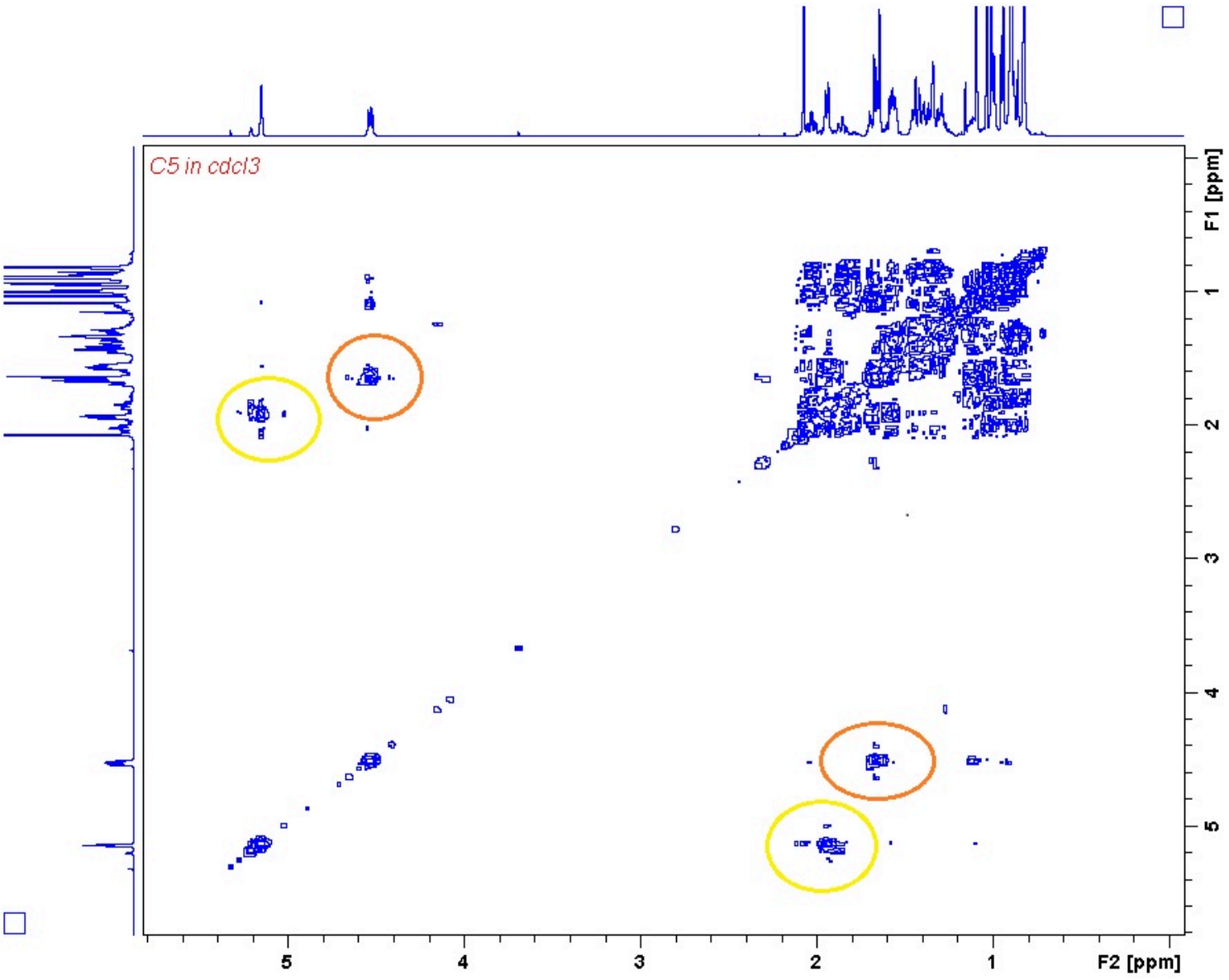

Figure 11

COSY spectrum of compound **C5** displaying ^{1}H - ^{1}H interactions **(**yellow circle: H-2 and H-3; red circle: H-11 and H-12).

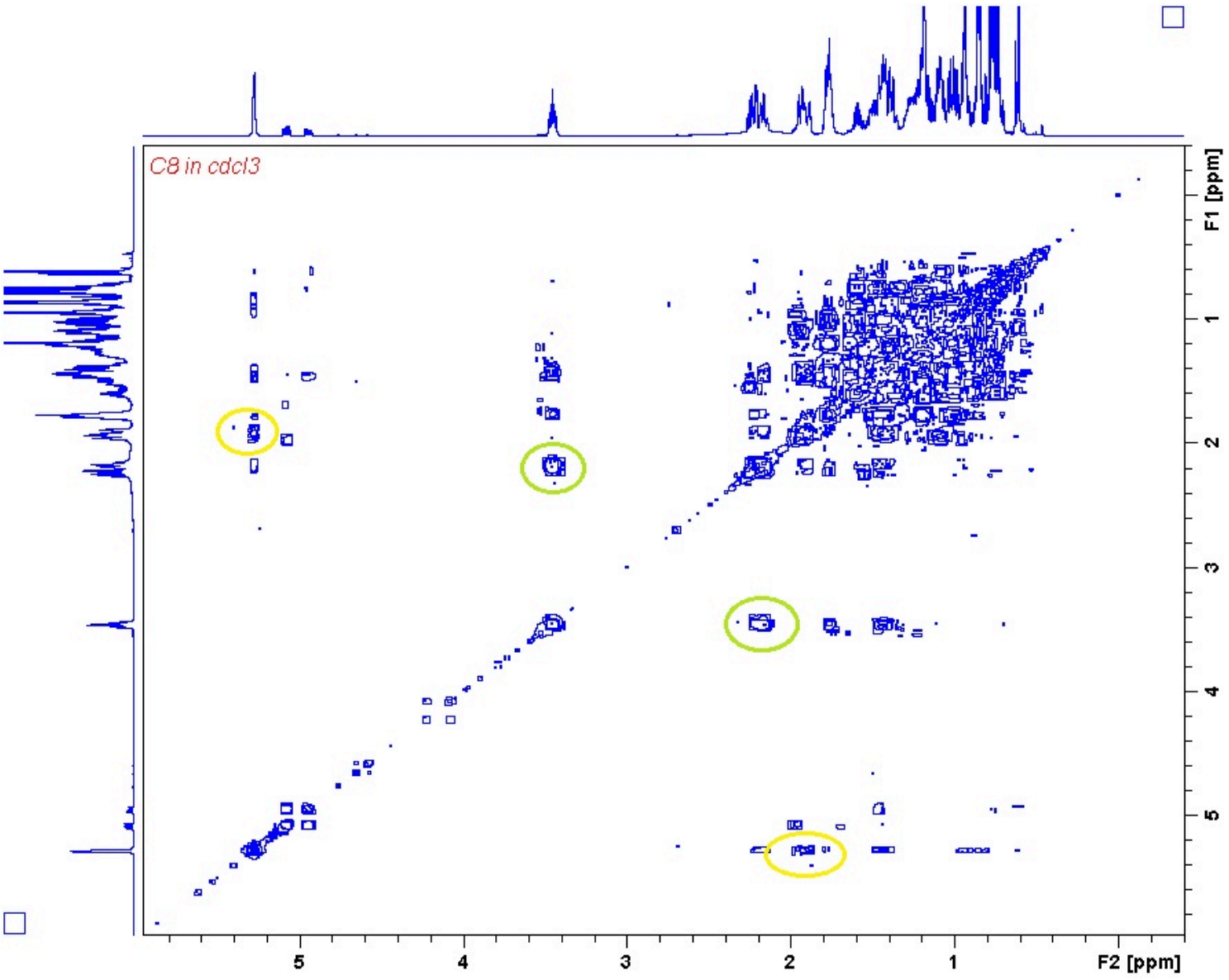

Figure 12

COSY spectrum of compound **C8** displaying ^{1}H - ^{1}H interactions (Green circle: H-2 and H-3; Yellow circle: H-6 and H-7).

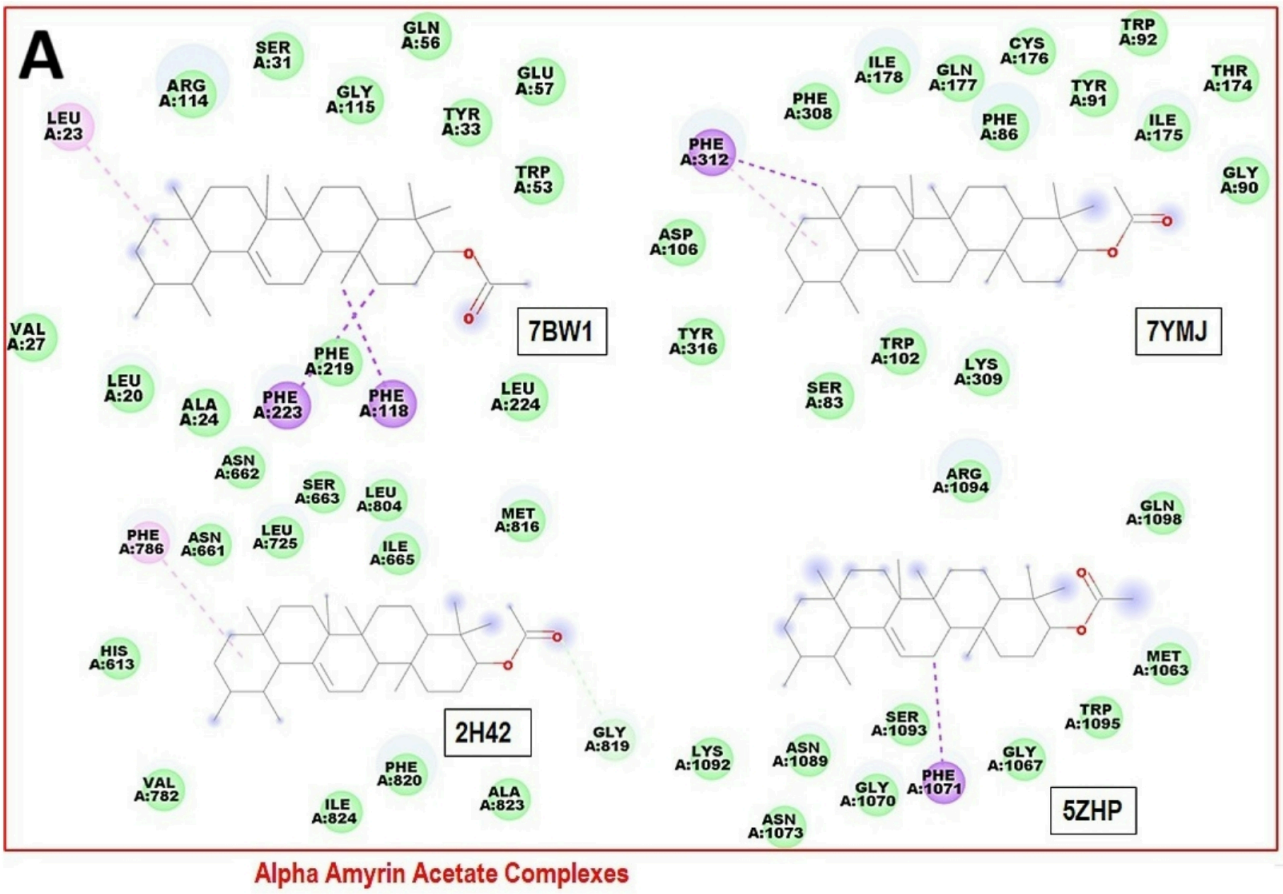

Figure 13

2D interaction map of α-amyrin acetate (A) complex with BPH target proteins - 5α-reductase type 2 (7BW1), α1A-adrenoceptor (7YMJ), phosphodiesterase-5 (2H42), and muscarinic M3 receptor (5ZHP).

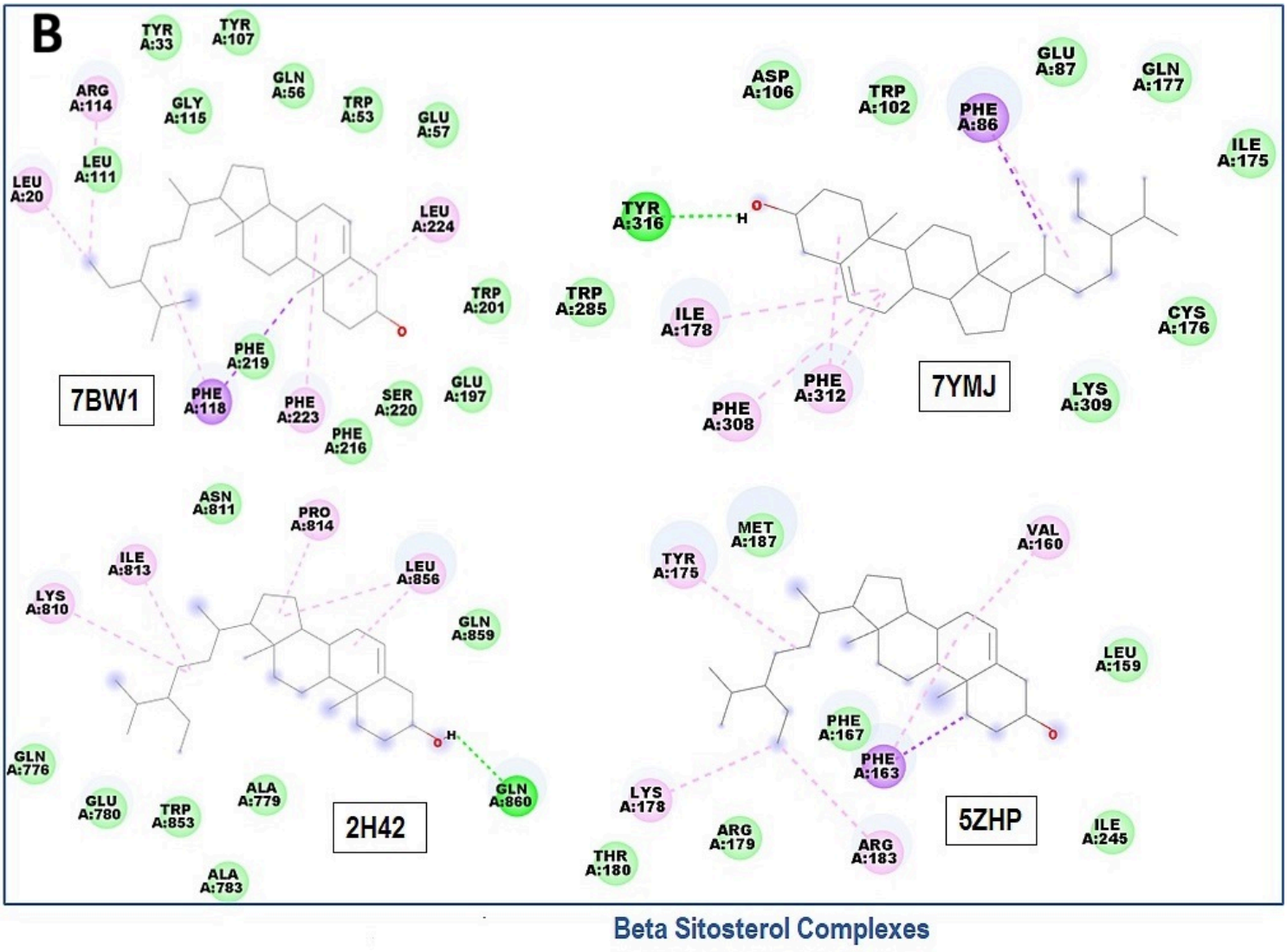

Figure 14

2D interaction map of β-sitosterol (B) complex with BPH target proteins - 5α-reductase type 2 (7BW1), α1A-adrenoceptor (7YMJ), phosphodiesterase-5 (2H42), and muscarinic M3 receptor (5ZHP).

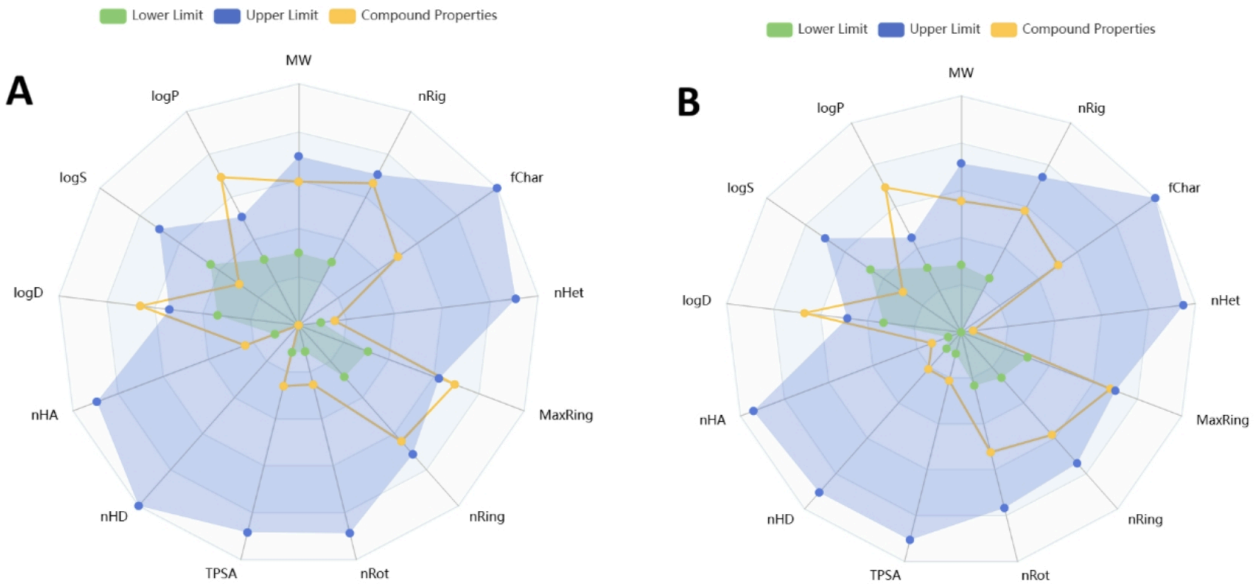

Figure 15

ADMETLab evaluation showing the suitable physicochemical space for oral bioavailability; A: α-amyrin acetate; B: β-sitosterol